Supplementary Information

Precisely Constructing Charge-Asymmetric Dual-Atom Fe Sites Supported on Hollow Porous Carbon Spheres for Efficient Oxygen Reduction

Yaqiong Li[+a], Xuan Luo[+b], Zihao Wei[+a], Fang Zhang[c], Zhiyi Sun[a], Ziwei Deng[a], Ziheng Zhan[a], Chaofeng Zhao[a], Qi Sun[a], Liang Zhang*[b], Wenxing Chen*[a], Shenghua Li*[a] and Siping Pang*[a]

[a.] Energy & Catalysis Center, School of Materials Science and Engineering, Beijing Institute of Technology, Beijing 100081, China, Email: wxchen@bit.edu.cn, lishenghua@bit.edu.cn, pangsp@bit.edu.cn

[b.] Center for Combustion Energy, School of Vehicle and Mobility, State Key Laboratory of Intelligent Green Vehicle and Mobility, Tsinghua University, Beijing 100084, China. Email: zhangbright@tsinghua.edu.cn

[c.] Analysis and Testing Center, Beijing Institute of Technology, Beijing Institute of Technology, Beijing 100081, P. R. China.

+ These authors contributed equally to this work.

Experimental Procedures

Materials

Styrene, Dopamine, $FeCl_3$, potassium persulfate, polyvinyl pyrrolidone (K40), thiourea, tris (Hydroxymethyl) aminomethane (tris), and bis (dicarbonylcyclopentadienyliron) (CDD) were purchase from Energy Chemical Co., Ltd. Other reagents were all analytical without further purification.

Preparation of PS spheres

The PS spheres were synthesized following a modified version of the reported procedure[1,2]. In a typical synthesis, 13 mL of styrene was thoroughly washed with a 10 wt.% NaOH solution, followed by rinsing with deionized water to remove the stabilizer. The washed styrene was then added to a triple-neck, 250 mL round-bottomed flask containing 100 mL of water, along with 0.5 g of PVP. To remove any remaining oxygen, the mixture was purged with nitrogen for 30 minutes. Subsequently, under magnetic stirring, the mixture was heated to a specified temperature and maintained for 30 minutes. Then, 5 mL of an aqueous solution containing 0.3 g of $K_2S_2O_8$ was quickly added to the flask to initiate the polymerization reaction of styrene. The stirring was continued for 24 hours at this temperature. After cooling, the resulting product appeared as a milk-like dispersion of monodispersed colloidal polystyrene spheres.

Preparation of Fe-N_4/NC

To prepare polydopamine-decorated PS spheres ($FeCl_3$/PS@DPA), 300 mg of PS spheres were dispersed in 100 mL of tris solution. Subsequently, 200 mg of dopamine hydrochloride and 4.8 mg (0.03 mmol) of $FeCl_3$ were added to the aforementioned solution under vigorous stirring for 20 hours. The resulting product was then washed with water and subsequently dried in an oven overnight. For the synthesis of Fe-N_4/NC, the $FeCl_3$/PS@DPA was subjected to heating at 800 °C for 2 hours in an N_2 atmosphere, with a ramping rate of 5 °C per minute.

Preparation of Fe-S_1N_3/SNC

300 mg PS sphere was first dispersed in 100 mL of tris solution, and then, 200 mg of dopamine hydrochloride, 4.8 mg (0.03 mmol) $FeCl_3$ and 10 mg thiourea were added to the above mentioned solution under vigorous stirring for 20 h to obtain polydopamine-decorated PS spheres (S/$FeCl_3$/PS@DPA); the product was then washed with water and then dried in an oven overnight. For the preparation of Fe-S_1N_3/SNC, S/$FeCl_3$/PS@DPA was heated at 800 °C for 2 h with a ramping rate of 5 °C per minute under an N_2 atmosphere.

Preparation of Fe_2-S_1N_5/SNC

To begin, 300 mg of PS spheres were dispersed in 100 mL of tris solution. Then, 5.3 mg (0.015 mmol) of CDD was dissolved in 2 mL of DMF and added to the aforementioned solution. Next, 200 mg of dopamine hydrochloride and 10 mg of thiourea were introduced into the mixture under vigorous stirring for 20 hours. This process resulted in the formation of polydopamine-decorated PS spheres (S/$FeCl_3$/PS@DPA). The product was subsequently washed with water and dried in an oven overnight. To synthesize Fe-S_1N_3/SNC, the S/$FeCl_3$/PS@DPA product was heated at 800 °C for 2 hours under an N_2 atmosphere, using a ramping rate of 5 °C per minute.

Electrochemical Characterizations

Electrochemical measurements were conducted using a CHI 760E electrochemical workstation (Shanghai Chenhua, China), employing a typical three-electrode configuration. A Pt wire served as the counter electrode and a Ag/AgCl electrode was used as the reference electrode. The working

electrode employed was a glassy carbon rotating disk electrode (GC-RDE) with a diameter of 5 mm. And, RRDE (disk outer diameter, ring inner diameter, and ring outer diameter are 5.61, 6.25, and 7.92 mm, respectively) was also used as working electrode for electrons transferred (n) and H_2O_2 yields. The electrolyte used was a 0.1 M $HClO_4$ solution. To prepare the catalyst ink, 3 mg of catalyst powder was dispersed in a 300 ul solution containing 147 μL of isopropyl alcohol, 147 μL of deionized water, and 6 μL of a 5% Nafion solution. This mixture was sonicated for at least 1 hour to ensure proper dispersion. Subsequently, 15 μL of the prepared catalyst ink was dropped onto a glassy carbon (GC) electrode. Prior to commencing measurements, the electrolyte in the cell was saturated with O_2 flow for 30 minutes to establish O_2-saturated conditions. The linear sweep voltammetry (LSV) experiments were conducted in O_2-saturated 0.1 M $HClO_4$. The LSV measurements of the catalysts were performed using the GC-RDE, with the rotation speed varying from 400 to 2500 rpm.

Electrochemical data processing

Tafel slopes $\eta = b \log (j/j_0)$, where η is the potential (V vs. RHE), b is the Tafel slope, j is the current density, and j_0 is the exchange current density. The kinetic current density (J_k) during ORR was calculated according to Koutecky-Levich equation:

$$\frac{1}{J} = \frac{1}{J_L} + \frac{1}{J_K} = \frac{1}{B\omega^{\frac{1}{2}}} + \frac{1}{J_K}$$

where J is the measured current density, J_K and J_L are the kinetic and limiting current densities, ω is the angular velocity of the disk.

The calculations of the transfer electron number (n) and the yield of H_2O_2 were derived from the RRDE measurement using the disk current (Id) and ring current (Ir), as determined by the following equations:

$$n = 4 \times \frac{I_d}{I_d + I_r / N}$$

$$H_2O_2\% = 200 \times \frac{I_r}{Ir + NI_d}$$

where N = 0.37 is the current collection efficiency of Pt ring.

MEA fabrication and fuel cell measurement

To fabricate the MEA, a mixture of 10 mg of catalyst and 200 mg of Nafion (5 wt %) was prepared by combining 500 μl of isopropanol and 250 μl of deionized water through sonication. The resulting catalyst ink was then applied to the carbon paper using a brush, with a cathode loading of 3 mg cm^{-2}. The anode, consisting of Pt/C (40 wt % of Pt), was prepared with a loading of approximately 0.4 mg_{Pt} cm^{-2}. The MEA was assembled by hot pressing the previously prepared cathode, anode, and a Nafion 212 membrane together at a temperature of 130°C for 120 seconds, under a pressure of 0.6 MPa. Subsequently, the PEMFC tests were conducted using an Arbin fuel cell test system, with the specified back pressure, operating at 80°C and 100% relative humidity.

DFT calculation

All calculations in this work were implemented in the Vienna ab initio simulation package (VASP) using density functional theory (DFT) methods[3,4]. Specifically, the projector augmented wave (PAW) method[5] was applied to treat electron-ion interactions, and the Perdew-Burke-

Ernzerhof (PBE) exchange–correlation functional within the generalized gradient approximation (GGA) employed to describe the electron interactions [6-8]. For the dispersion interaction, the van der Waals correction was performed in DFT-D3 method [9,10]. The energy cutoff for the plane-wave basis was adopted as 520 eV. All atoms are relaxed using a 2×3×1 Monkhorst−Pack [11] k-point mesh during the geometric optimization, where the force and energy convergence criteria are set to 0.025 eV/Å and 10^{-5} eV, respectively. A graphene supercell containing 86/90 C atoms were employed to construct Fe single-/double- atom moieties coordinated in three distinct environments (denoted herein as Fe_2-S_1N_5/SNC, Fe-S_1N_3/SNC, and Fe-N_4/NC, where Fe is the centre and N and S are atoms bonded directly to the Fe centre. Each moiety is supported by carbon), as shown in Fig. Sx. To avoid interaction between periodic images, a vacuum space of 20 Å was created in the z direction. In structural relaxation, all atoms are allowed to relax.

The adsorption energies (E_{ads}) were calculated as:

$$\Delta E_{ads} = E_{ad/sub} - E_{ad} - E_{sub}$$

where $E_{ad/sub}$, E_{ad}, and E_{sub} are the total energies of the optimized adsorbate-substrate system, the adsorbate in the gas phase, and the clean substrate, respectively. The free energies of elemental reaction steps were calculated by the computational hydrogen electrode model developed by Nørskov et al.[12]. The free energy (ΔG) for elemental reaction step were calculated as:

$$\Delta G = \Delta E_{ads} + \Delta E_{ZPE} - T\Delta S$$

where ΔE_{ZPE} and ΔS are the differences in the zero-point energy and the change of entropy, T is the temperature (T =298 K in this work), respectively.The four elementary steps of ORR are defined as ΔG_i (i = 1–4) The overpotential of ORR (η_{ORR}) can be written as:

$$\eta_{ORR} = \frac{max\{\Delta G_1, \Delta G_2, \Delta G_3, \Delta G_4\}}{e} + 1.23$$

XAFS measurements

The radiation was monochromatized by a Si (111) double-crystal monochromator. The intensity of the incident X-ray was monitored by an N_2-filled ion chamber (I_0) in front of the sample. Solid samples were placed in an aluminum sample holder sealed with kapton tape. Data were collected as fluorescence excitation spectra with a Lytle detector. All data were collected at room temperature.

XAFS data processing

The acquired EXAFS data were processed according to the standard procedures using the Athena and Artemis implemented in the IFEFFIT software packages. The fitting detail is described below:

The acquired EXAFS data were processed according to the standard procedures using the ATHENA module implemented in the IFEFFIT software packages. The EXAFS spectra were obtained by subtracting the post-edge background from the overall absorption and then normalizing with respect to the edge-jump step. Subsequently, the $\chi(k)$ data of were Fourier transformed to real (R) space using a hanning windows (dk=1.0 $Å^{-1}$) to separate the EXAFS contributions from different coordination shells. To obtain the quantitative structural parameters around central atoms, least-squares curve parameter fitting was performed using the ARTEMIS module of IFEFFIT software packages.

The following EXAFS equation was used:

$$\chi(k)=\sum_j \frac{N_j S_o^2 F_j(k)}{k R_j^2}\exp[-2k^2\sigma_j^2]\exp[\frac{-2R_j}{\lambda(k)}]\sin[2kR_j+\phi_j(k)]$$

S_0^2 is the amplitude reduction factor, $F_j(k)$ is the effective curved-wave backscattering amplitude, N_j is the number of neighbors in the j^{th} atomic shell, R_j is the distance between the X-ray absorbing central atom and the atoms in the j^{th} atomic shell (backscatterer), λ is the mean free path in Å, $\phi_j(k)$ is the phase shift (including the phase shift for each shell and the total central atom phase shift), σ_j is the Debye-Waller parameter of the j^{th} atomic shell (variation of distances around the average R_j). The functions $F_j(k)$, λ and $\phi_j(k)$ were calculated with the ab initio code FEFF8.2. The coordination numbers of model samples were fixed as the nominal values. The obtained S_0^2 was fixed in the subsequent fitting. While the internal atomic distances R, Debye-Waller factor σ^2, and the edge-energy shift ΔE_0 were allowed to run freely.

Figures

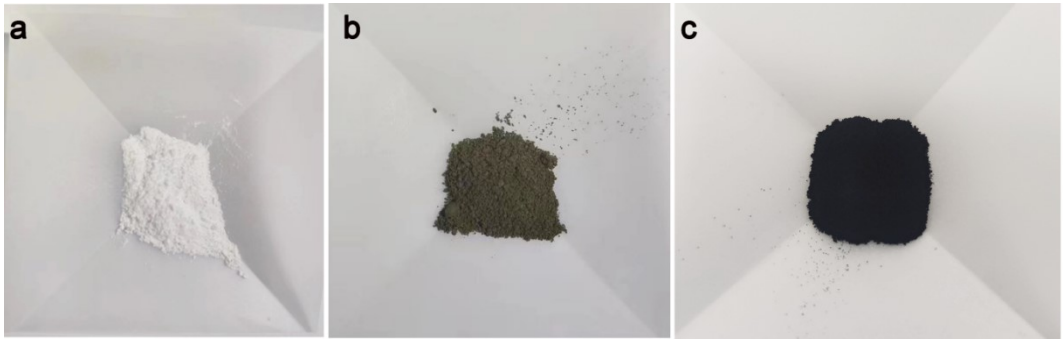

Figure S1 Digital photographs of (a) PS spheres, (b) shore-shell S/CDD/PS@PDA and (c) Fe_2-S_1N_5/SNC, respectively.

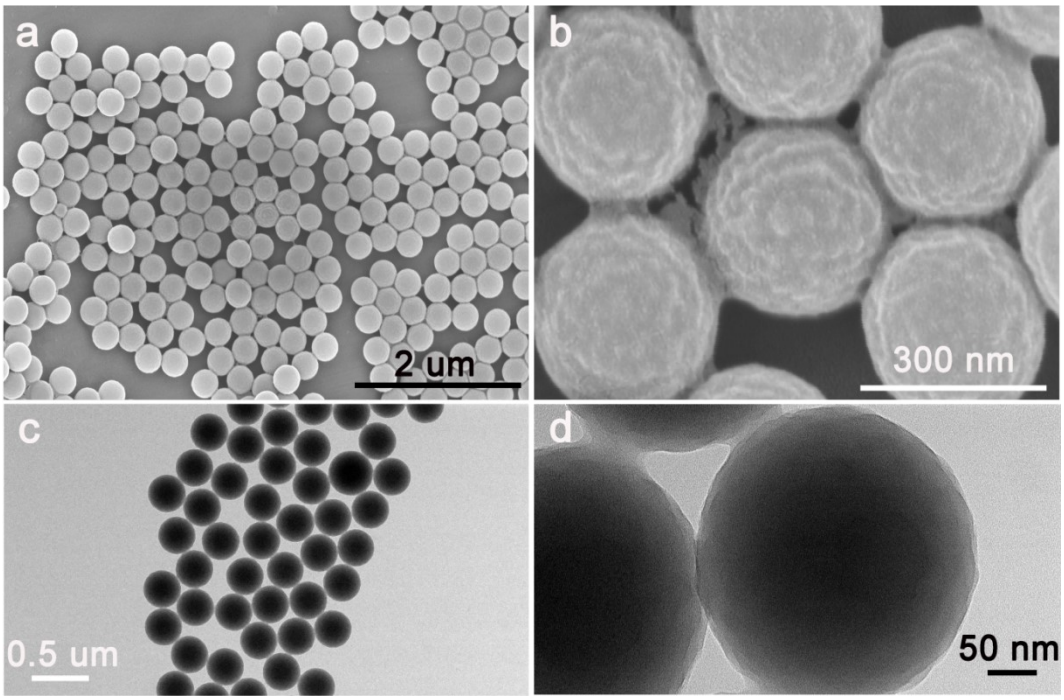

Figure S2 The morphology structures of the PS spheres. (a) and (b) SEM with different magnification. (c) and (d) TEM with different magnification.

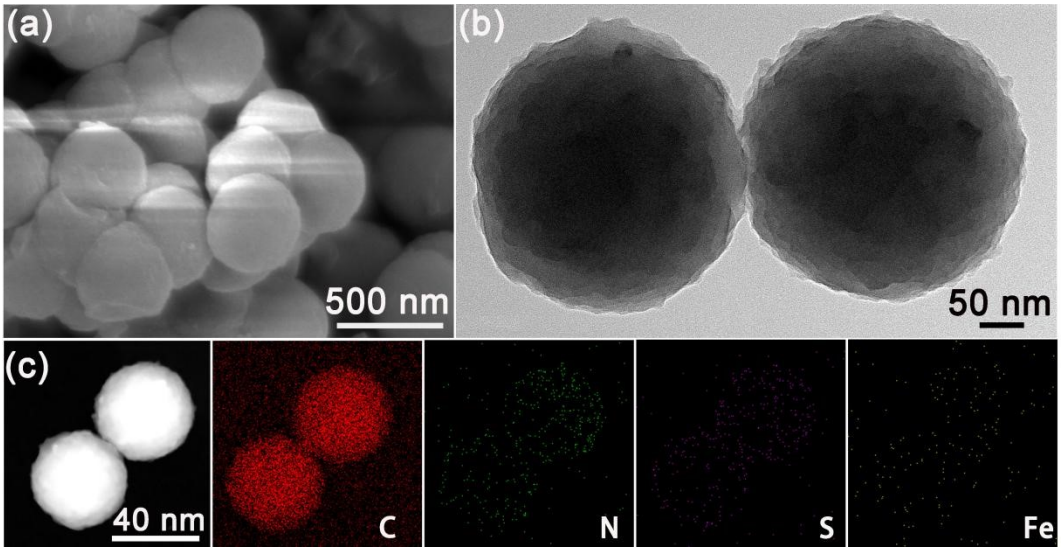

Figure S3 The morphology structures of the shore-shell S/CDD/PS@PDA. (a) SEM. (b) TEM. (c) EDS mappings of S/CDD/PS@PDA with mappings of individual elements (C, N, S and Fe).

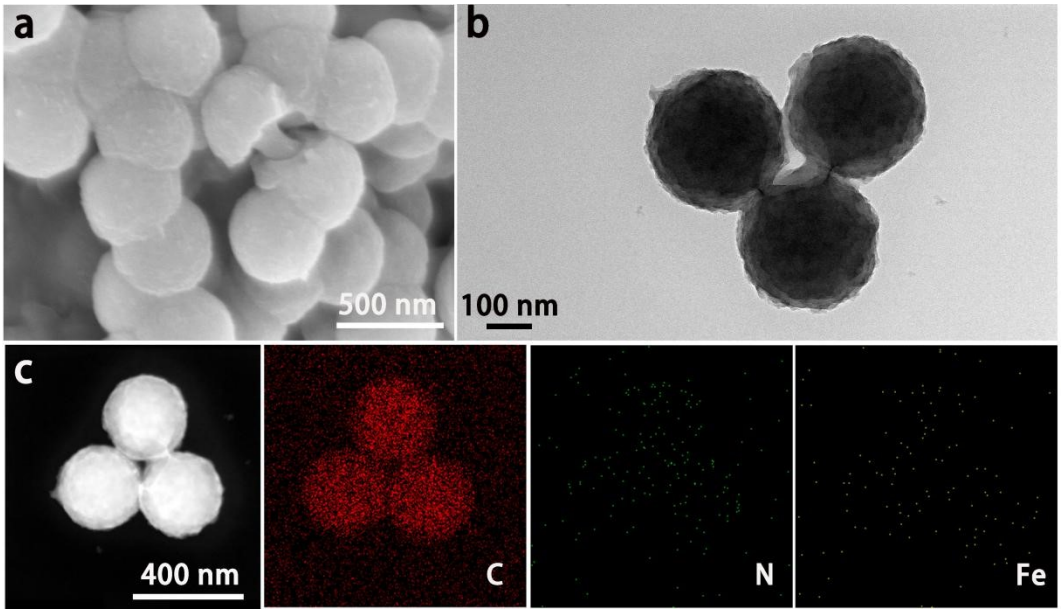

Figure S4 The morphology structures of the shore-shell $FeCl_3$/PS@PDA. (a) SEM. (b) TEM. (c) EDS mappings of $FeCl_3$/PS@PDA with mappings of individual elements (C, N, and Fe).

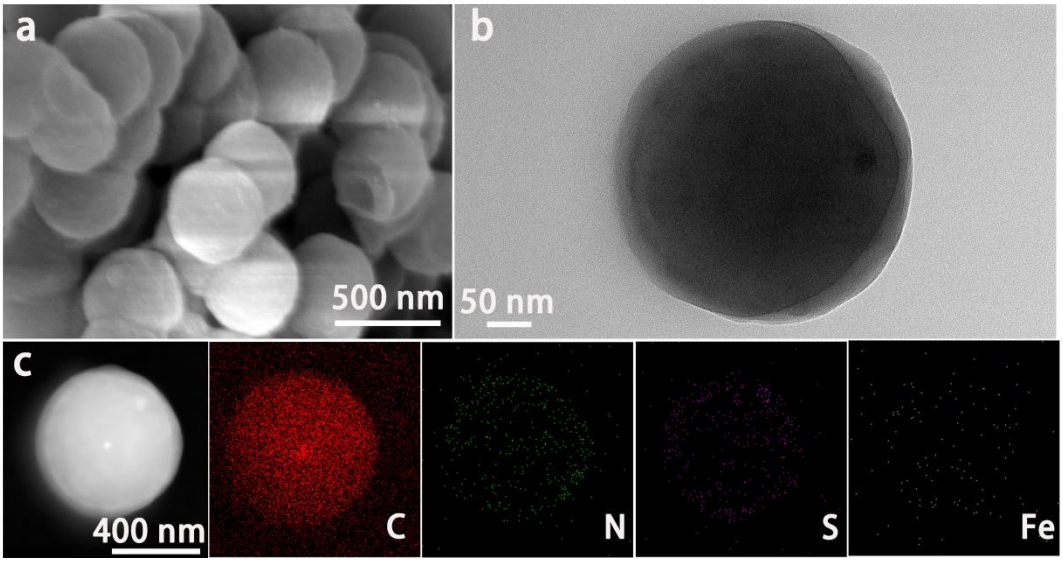

Figure S5 The morphology structures of the shore-shell S/$FeCl_2$/PS@PDA. (a) SEM. (b) TEM. (c) EDS mappings of S/$FeCl_3$/PS@PDA with mappings of individual elements (C, N, S and Fe).

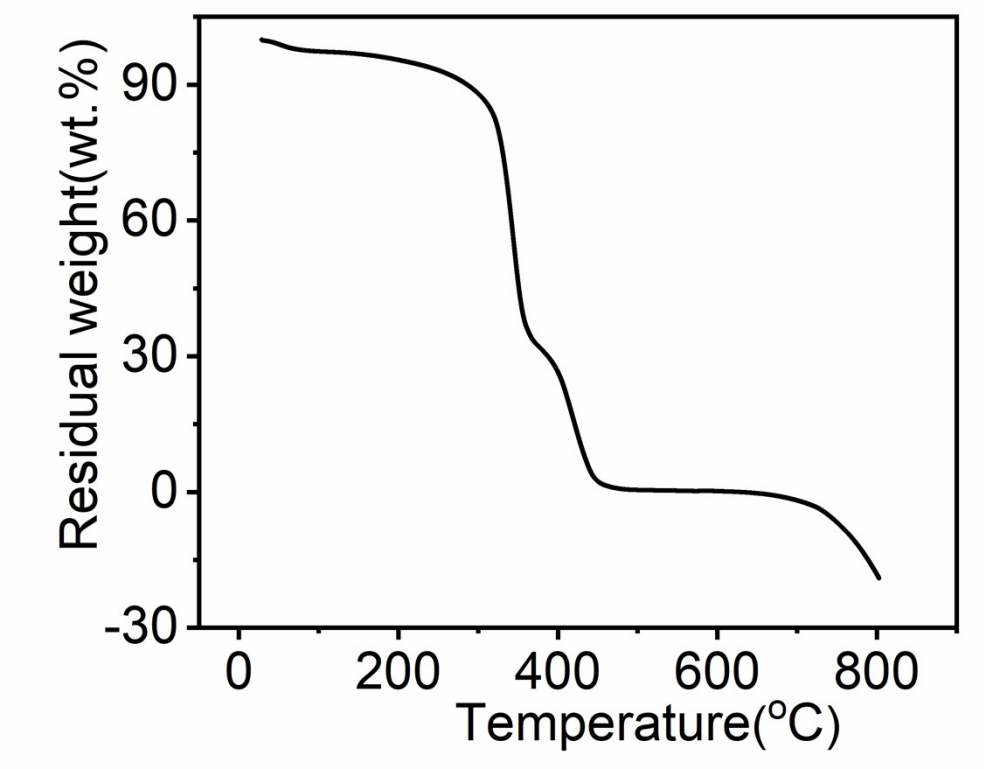

Figure S6 The TG thermal analysis of S/CDD/PS@PDA.

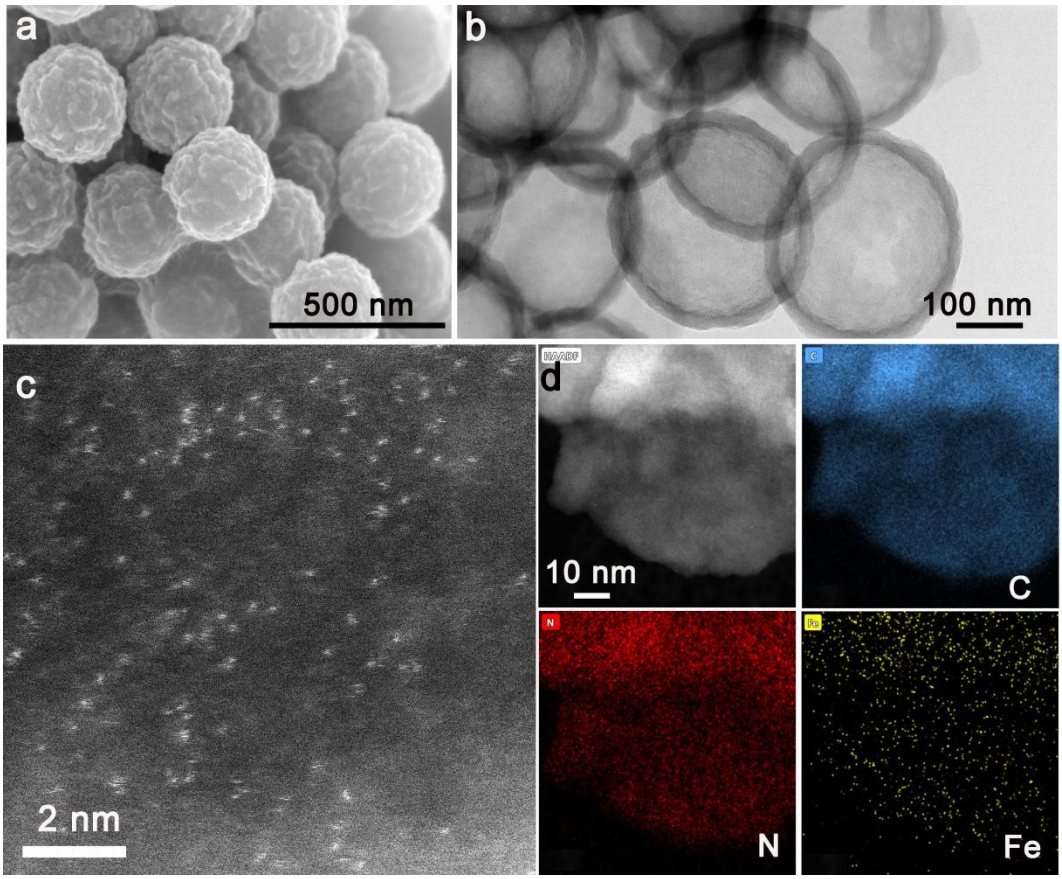

Figure S7 The morphology structures of the hollow Fe-N_4/NC. (a) SEM. (b) TEM. (c) HAADF-STEM image. (d) EDS mappings of Fe-N_4/NC with mappings of individual elements (C, N and Fe).

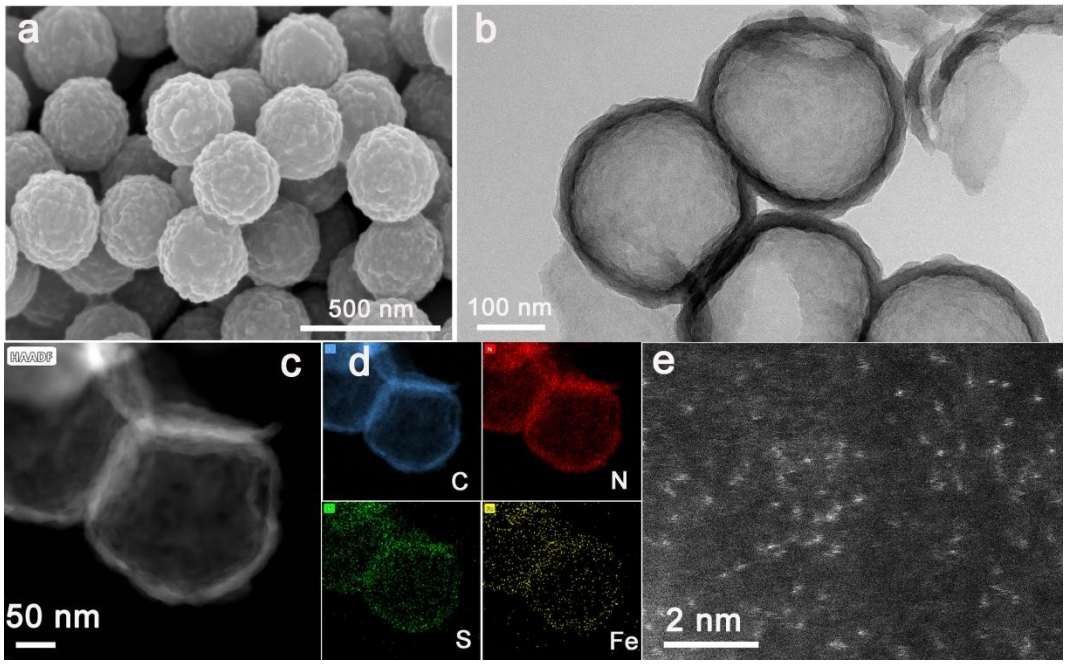

Figure S8 The morphology structures of the hollow Fe-S_1N_3/SNC. (a) SEM. (b) TEM. (c) HAADF-STEM image. (d) EDS mappings of Fe-S_1N_3/SNC with mappings of individual elements (C, N, S and Fe).

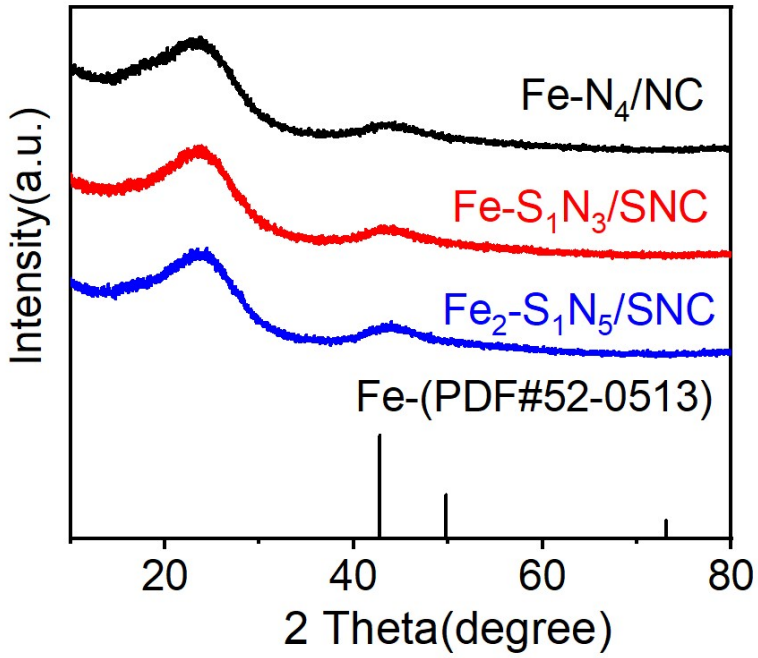

Figure S9 XRD patterns of Fe-N_4/NC, Fe-S_1N_3/SNC, and Fe_2-S_1N_5/SNC catalysts. For all atomic catalysts, one peak at the range of 20-30° assigned to the (002) plane of the graphitic carbon, and another broadened peak at the range of 40-50°assigned to the (101) plane of the graphitic carbon.

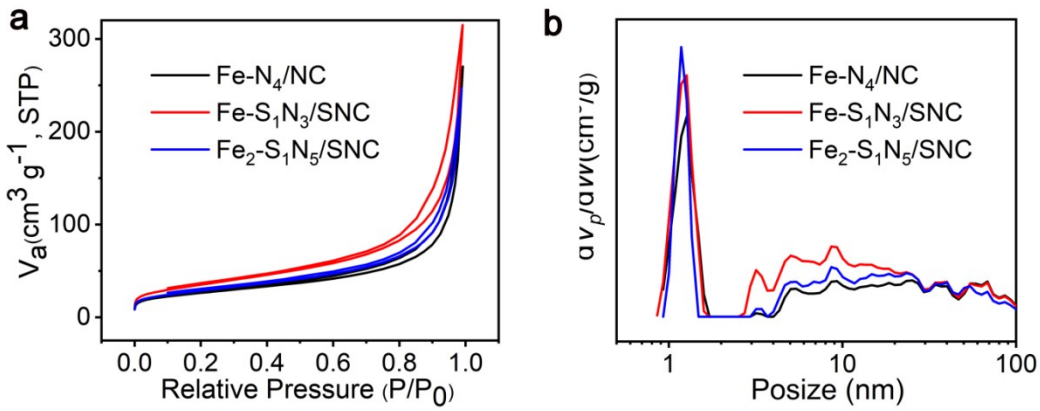

Figure S10 (a)The N_2 adsorption and desorption isotherm and (b)pore-size distribution curves of Fe-N_4/NC, Fe-S_1N_3/SNC, Fe_2-S_1N_5/SNC.

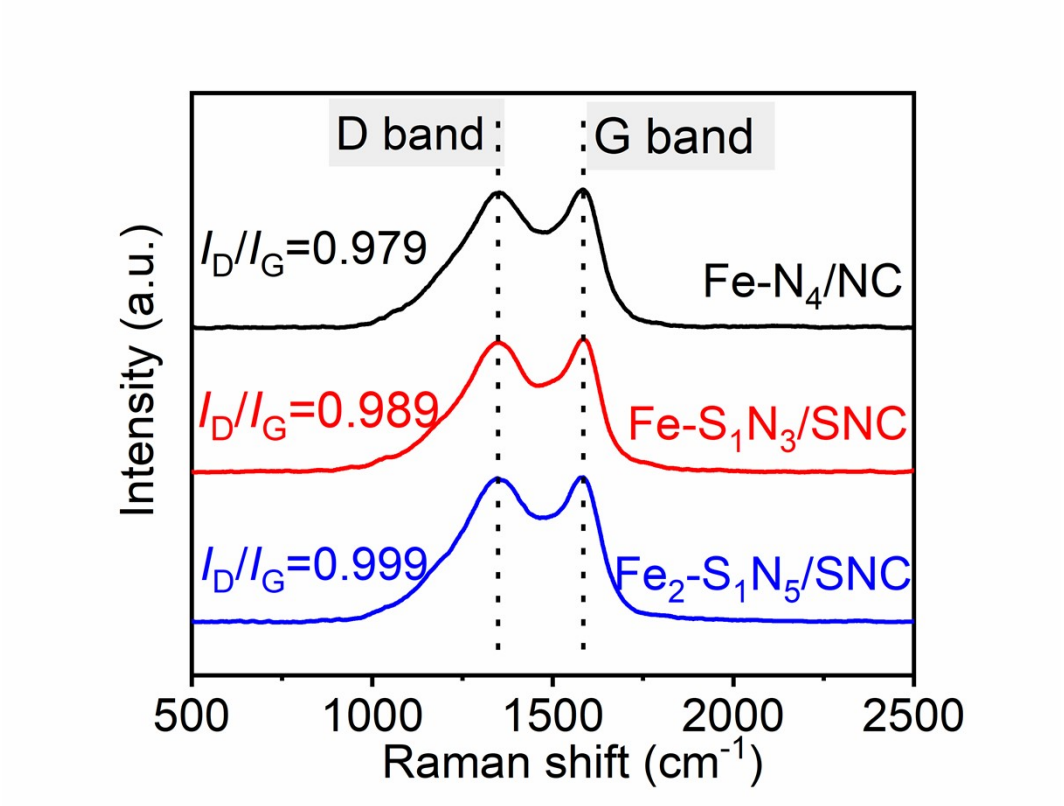

Figure S11 The Raman spectra of Fe-N_4/NC, Fe-S_1N_3/SNC and Fe_2-S_1N_5/SNC catalysts.

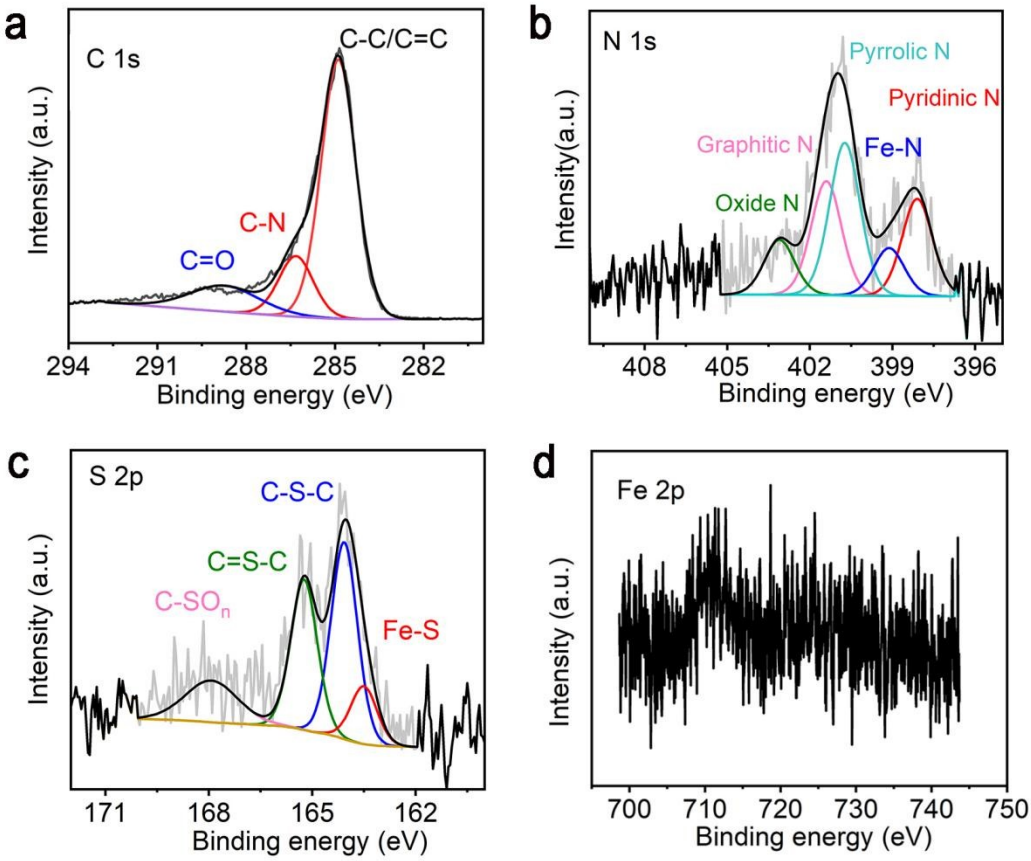

Figure S12 XPS spectra for Fe_2-S_1N_5/SNC. The XPS spectra for the (a) C 1s, (b) N 1s, (c) S 2p and (d) Fe 2p region.

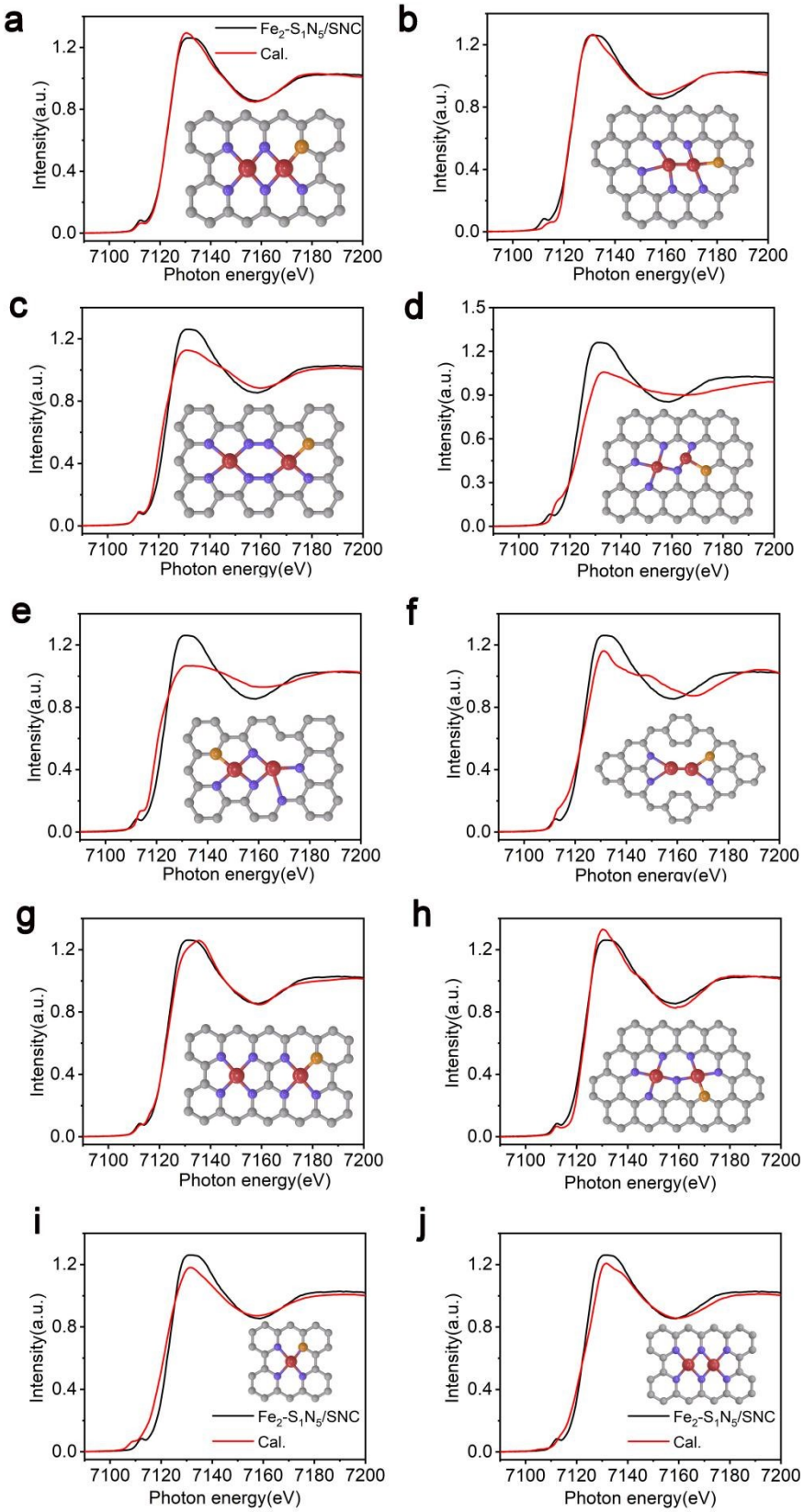

Figure S13 Model Comparison between the K-edge XANES experimental spectra of Fe_2-S_1N_5/SNC (black lines) and the theoretical spectra calculated with the depicted structures (red lines).

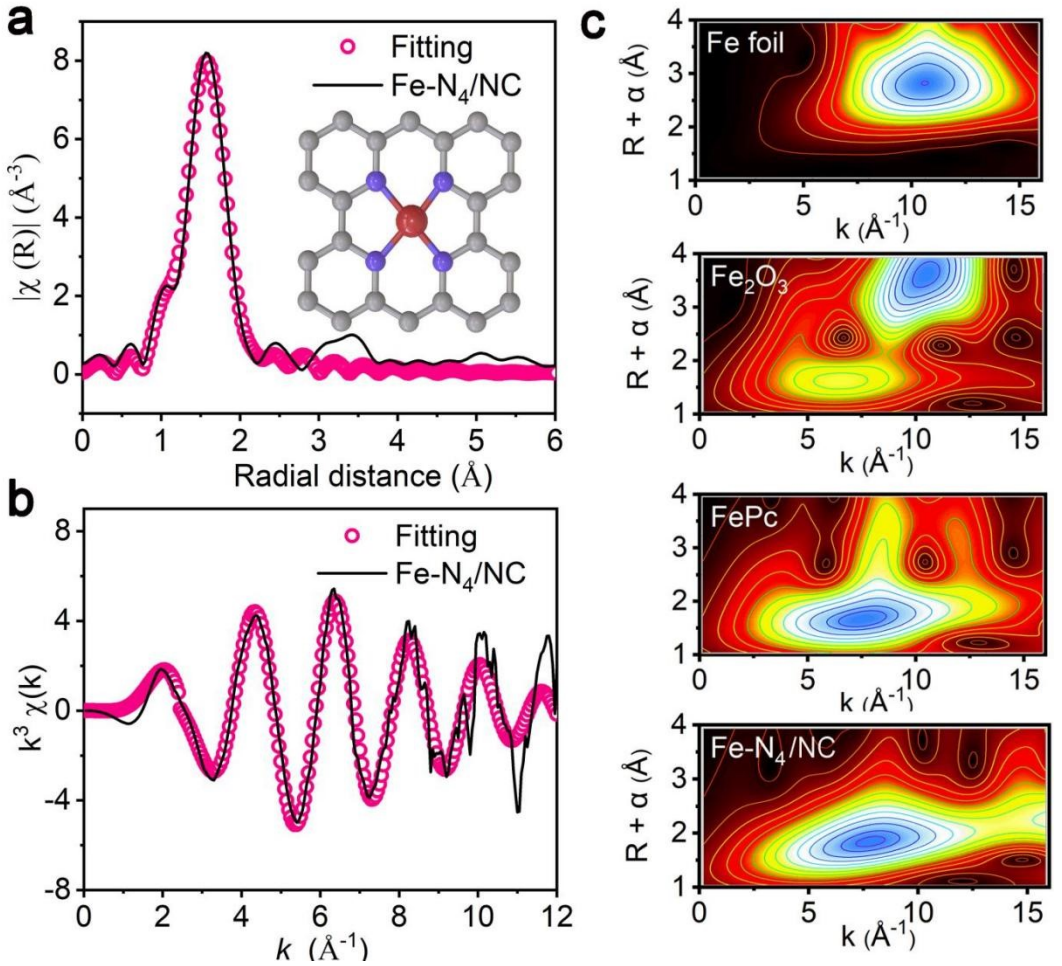

Figure S14 X-ray absorption analysis. (a) EXAFS fitting of Fe-N_4/NC in R space at Fe K-edge. The insets are structure model of the Fe-N_4/NC (Fe in purple, N in blue, and C in gray). (b) EXAFS fitting of Fe-N_4/NC in Kspace at Fe K-edge. (c) Fe K-edge WT-EXAFS contour plots for Fe-N_4/NC and reference samples.

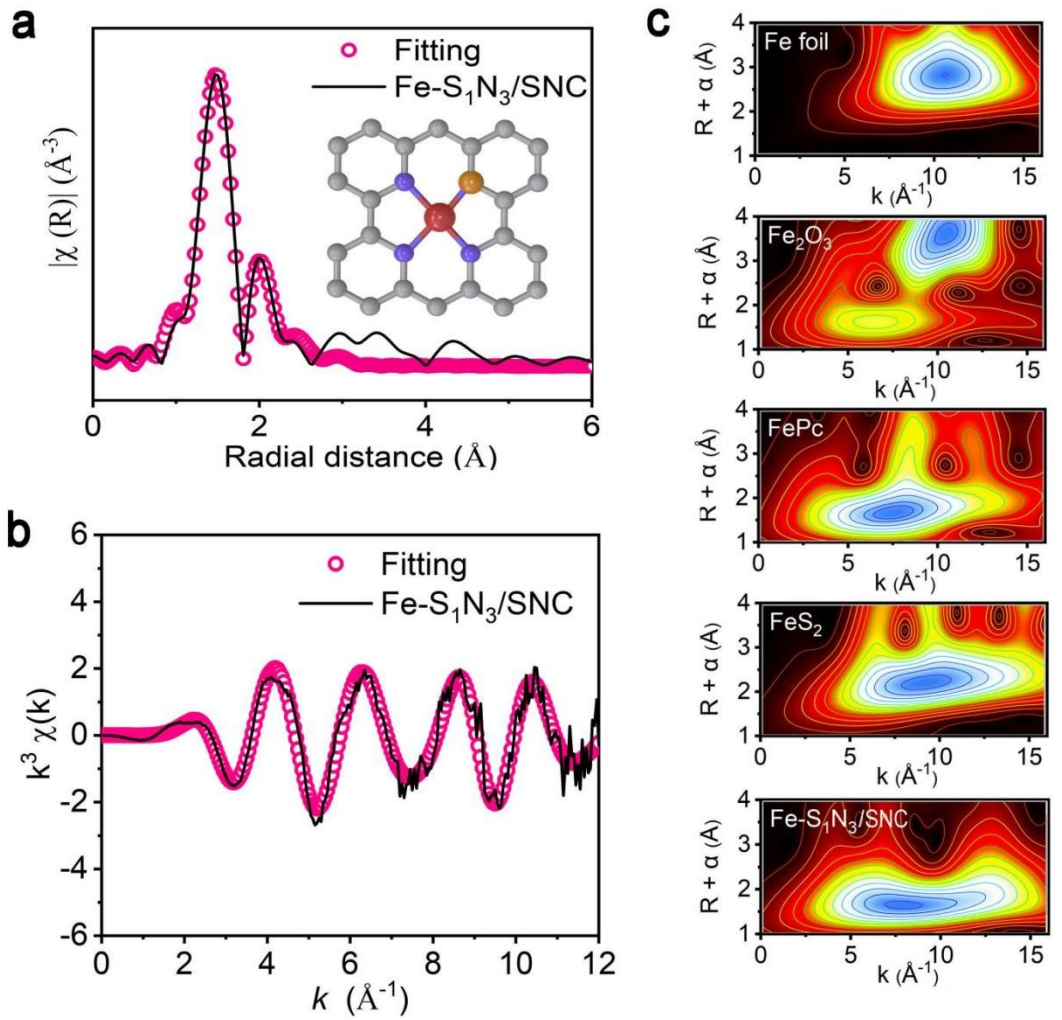

Figure S15 X-ray absorption analysis. (a) EXAFS fitting of Fe-S_1N_3/SNC in R space at Fe K-edge. The insets are structure model of the Fe-S_1N_3/SNC (Fe in purple, N in blue, S in yellow, and C in gray). (b) EXAFS fitting of Fe-S_1N_3/SNC in Kspace at Fe K-edge. (c) Fe K-edge WT-EXAFS contour plots for Fe-S_1N_3/SNC and reference samples.

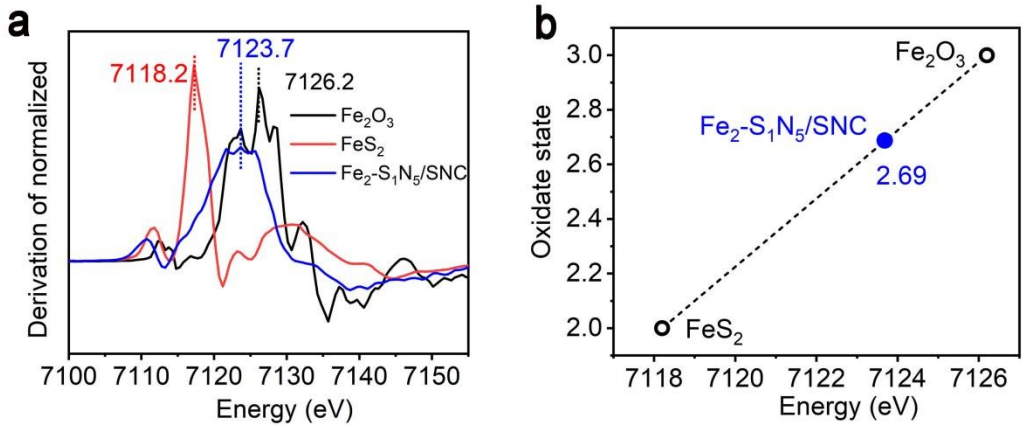

Figure S16 Characterization of Fe oxidation state from XANES. (a) First-derivative curves of Fe_2-S_1N_5/SNC and the references. (b) Correlation between the Fe oxidation state and the energy position of the XANES spectrum, determined as the first maximum of the first derivative spectrum of Fe_2-S_1N_5/SNC and different ion reference compounds.

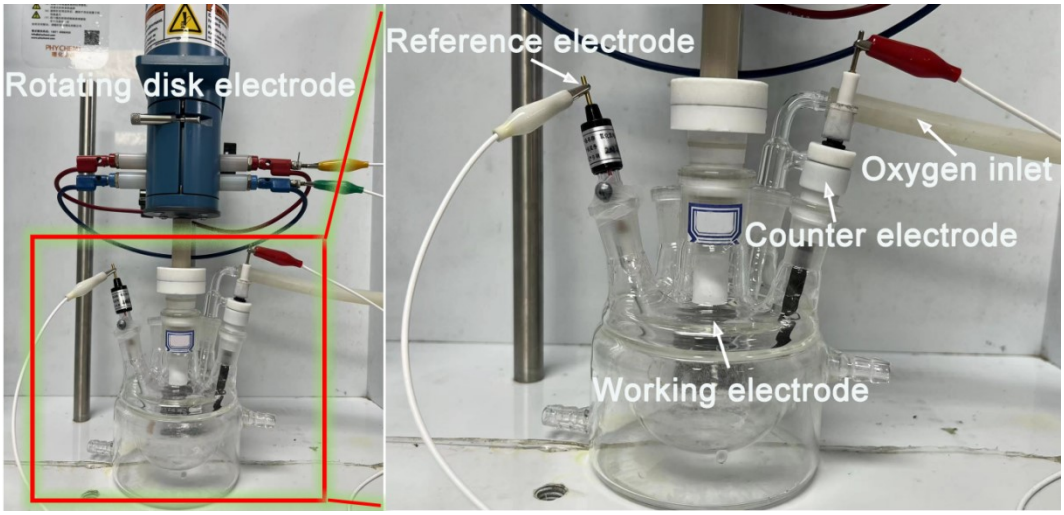

Figure S17 Photograph of the typical three-electrode setup for the electrochemical ORR measurements.

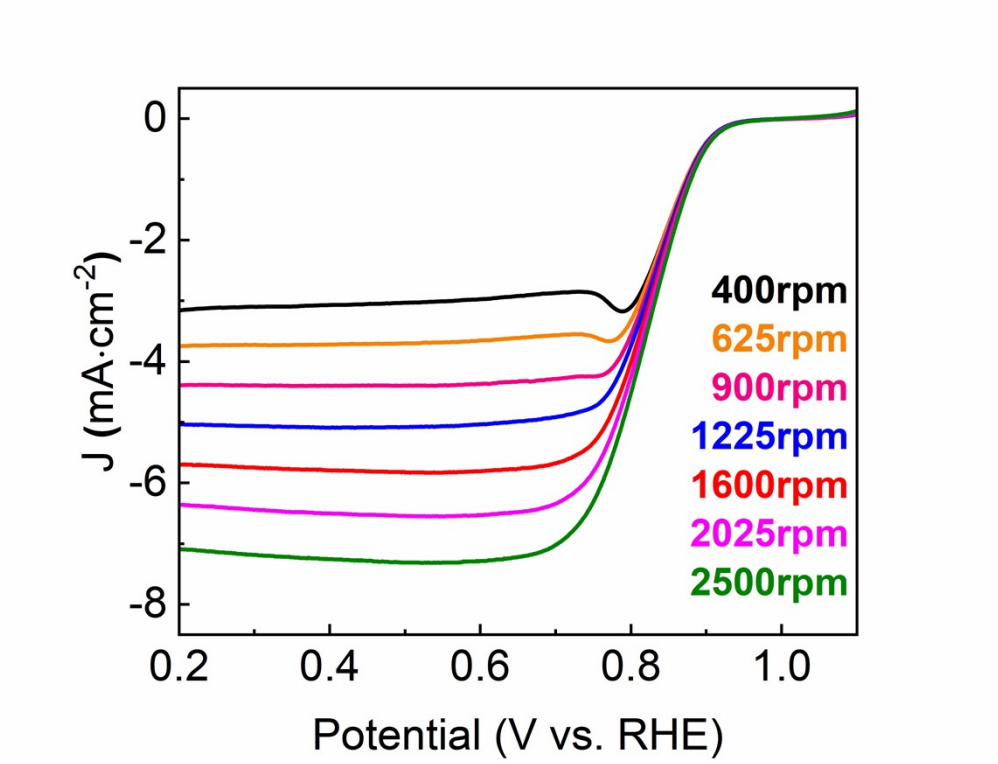

Figure S18 The ORR polarization curves of Fe_2-S_1N_5/SNC at different rotating rates.

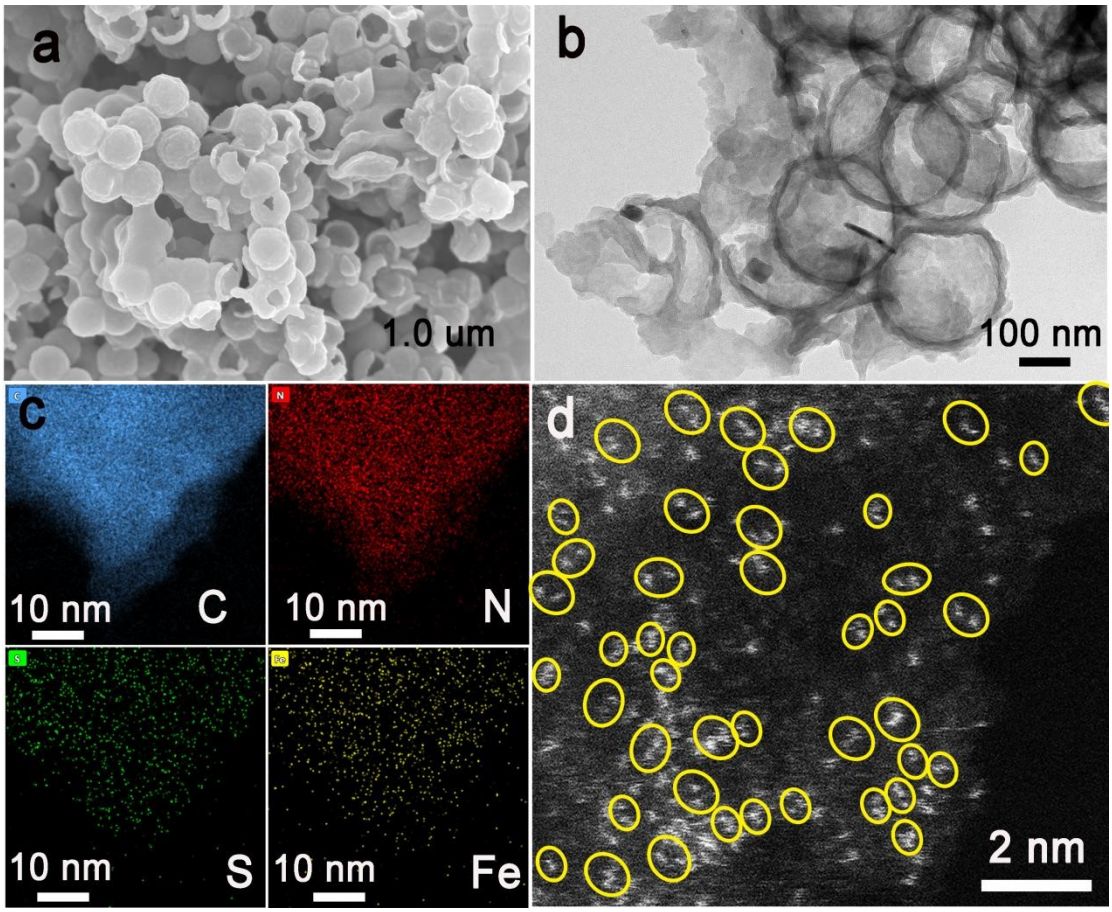

Figure S19 Morphology characterizations of Fe_2-S_1N_5/SNC catalyst after durability test. (a) SEM. (b) TEM. (c) EDS mapping. (d) HAADF-STEM images.

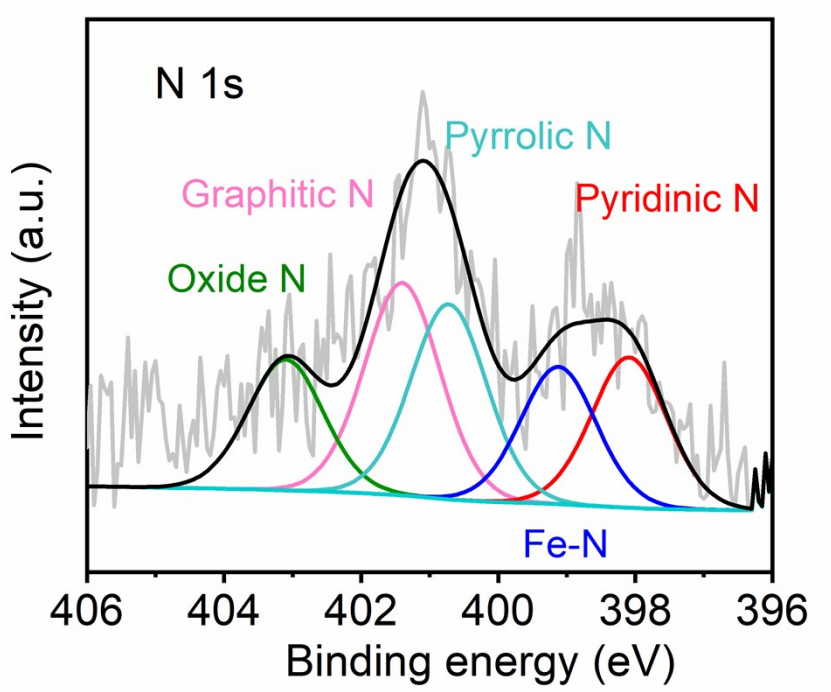

Figure S20 N 1s XPS results of Fe_2-S_1N_5/SNC after durability test.

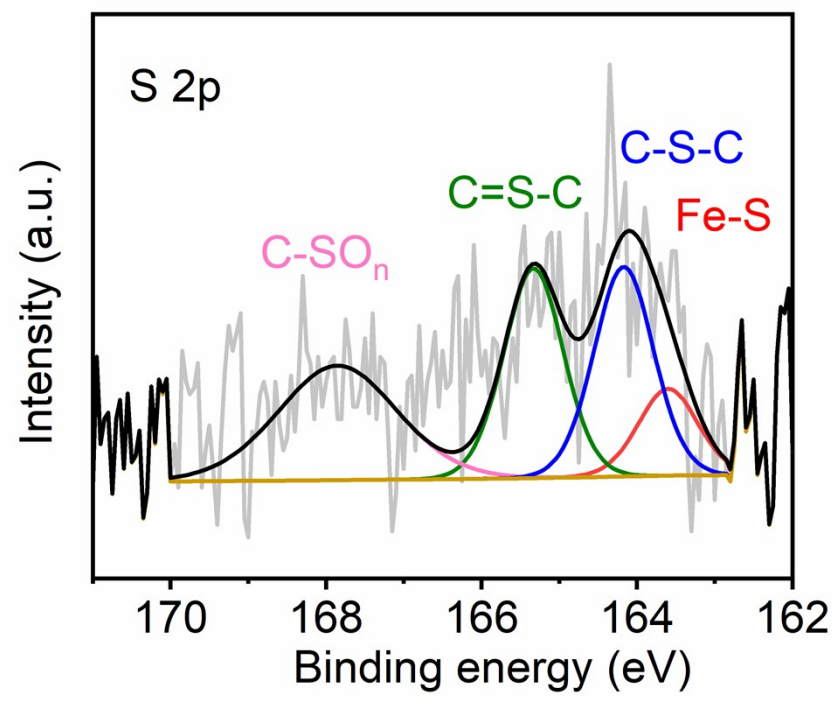

Figure S21 S 2p XPS results of Fe_2-S_1N_5/SNC after durability test.

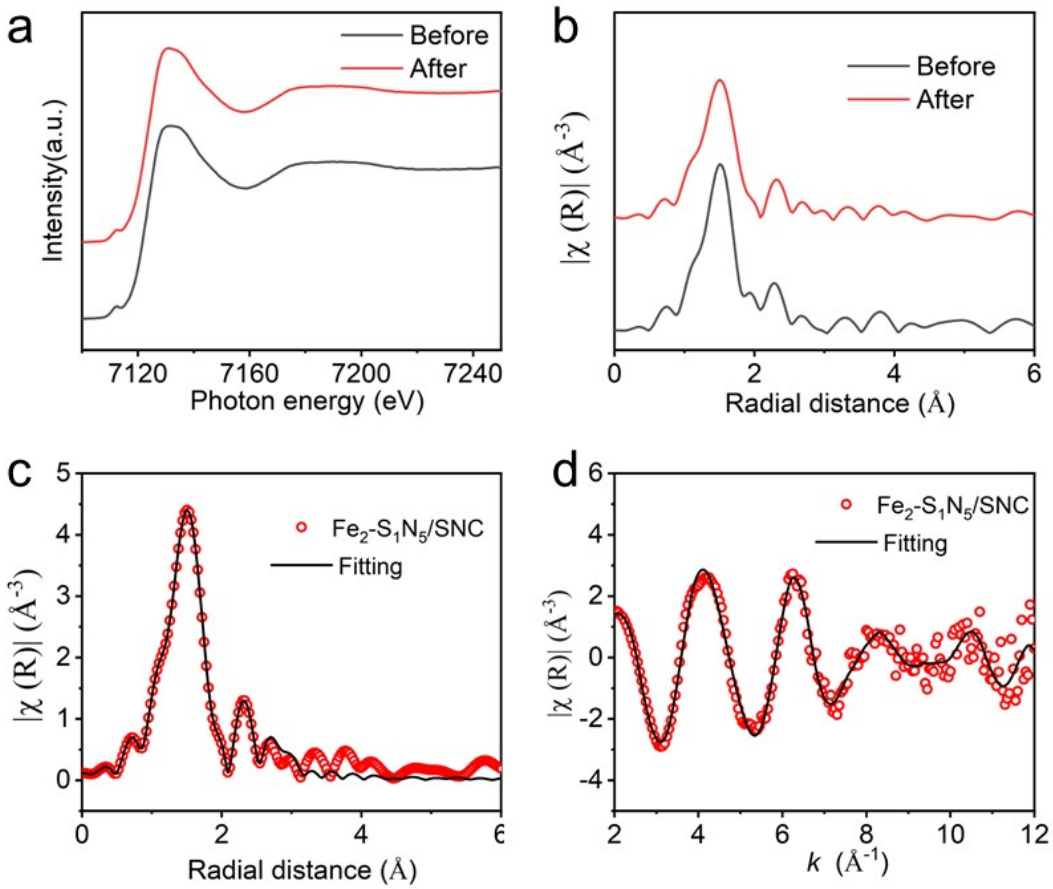

Figure S22 XANES spectra of the Fe_2-S_1N_5/SNC. (a) Fe K-edg before and after ORR reaction. (b) Fourier transforms of extended X-ray absorption fine structure (EXAFS) spectra of Fe K-edge before and after ORR reaction. (c) EXAFS fitting of Fe_2-S_1N_5/SNC in R space at Fe K-edge after ORR reaction. (d) EXAFS fitting of Fe_2-S_1N_5/SNC in K space at Fe K-edge after ORR reaction.

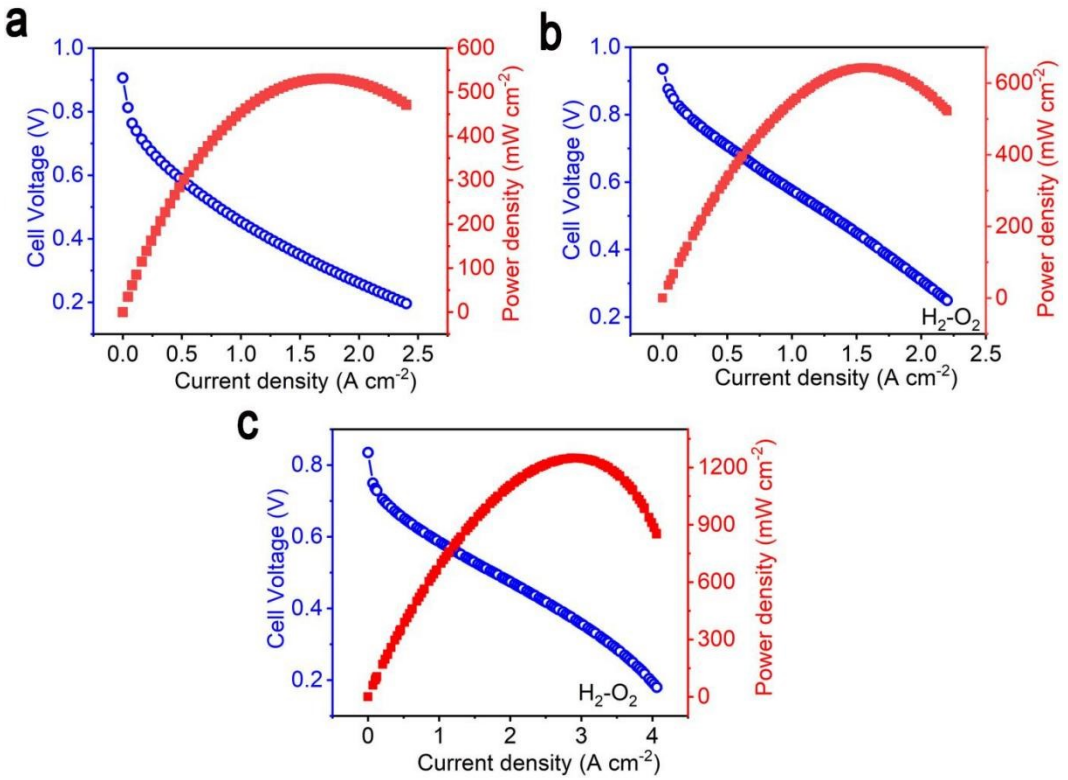

Figure S23 PEMFC polarization and power density curves of various catalysts. Test conditions: cathode loading of 3 mg cm^{-2} for relative catalysts, anode loading of 0.4 mg_{Pt} cm^{-2} for Pt/C, 2 bar H_2/O_2. (a) Fe-N_4/NC. (b) Fe-S_1N_3/SNC. (c) Pt/C.

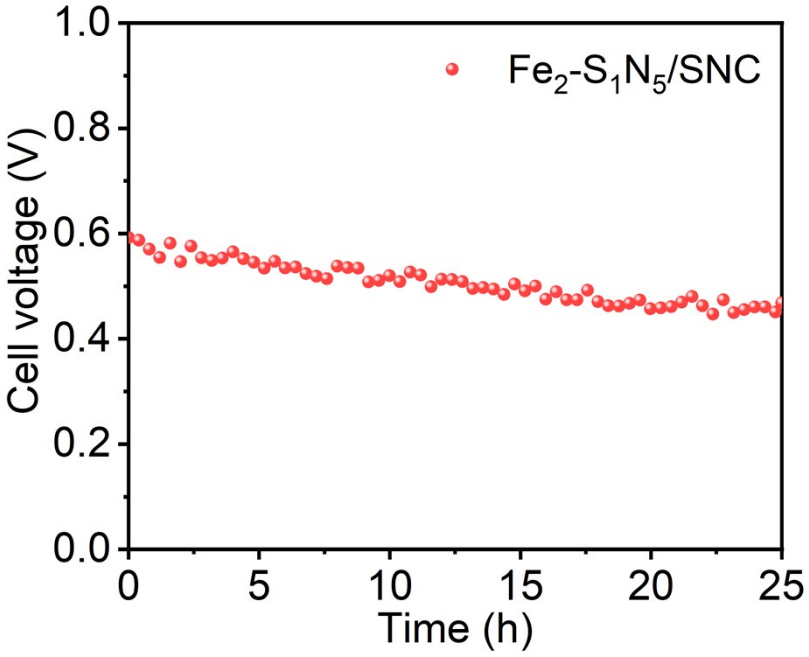

Figure S24 The stability of PEMFC with Fe_2-S_1N_5/SNC as cathode at a density of 1 A cm^{-2}.

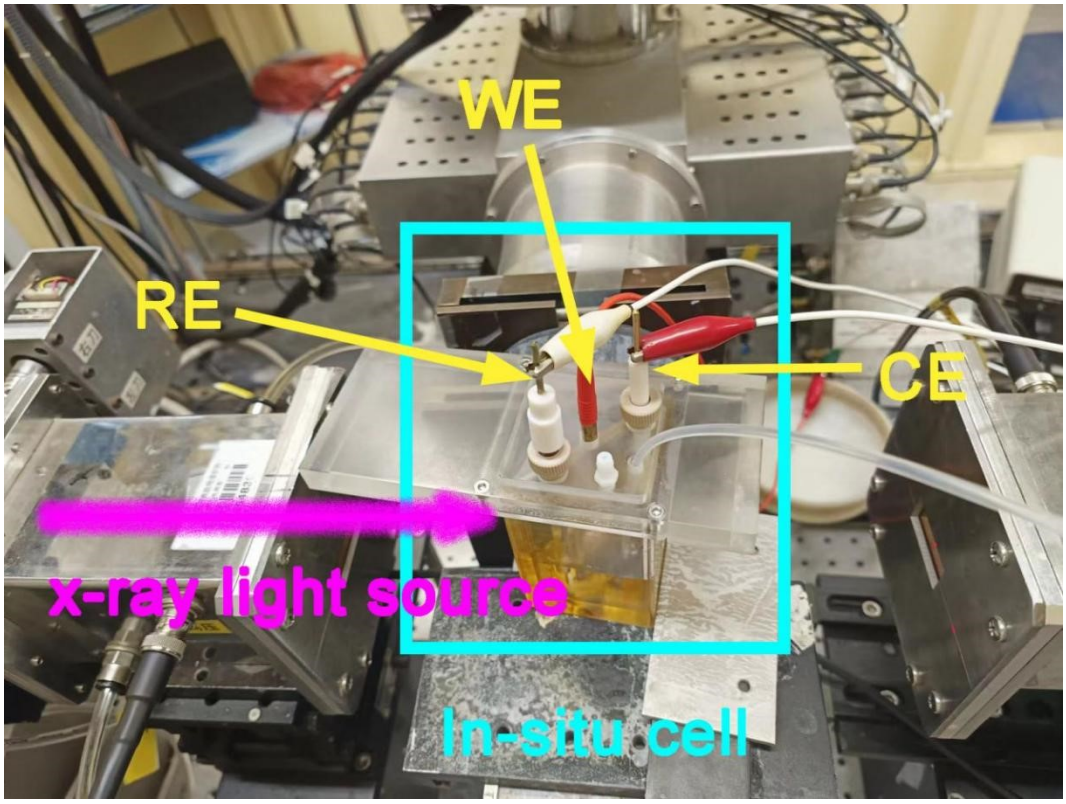

Figure S25 The detail of the in-situ X-ray absorption spectroscopy measurement. CE, counterelectrode; WE, working electrode; RE, reference electrode.

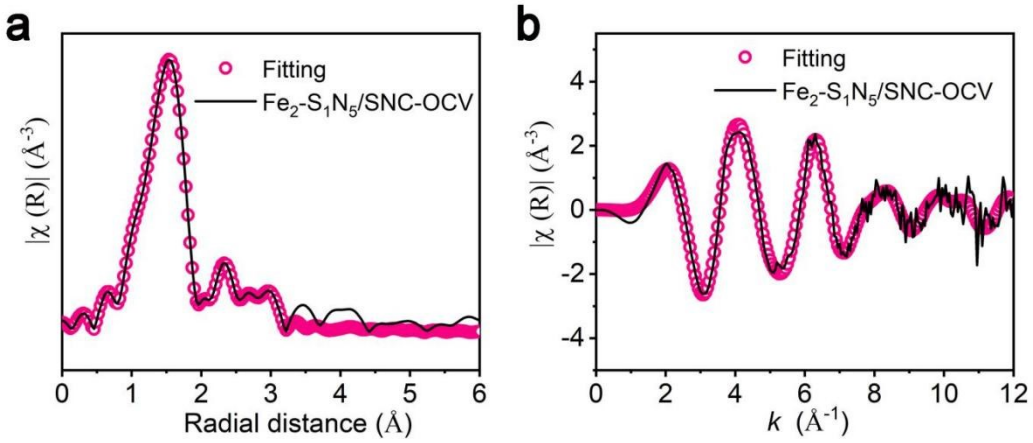

Figure S26 EXAFS fitting at OCV. (a) The EXAFS fitting in R space at Fe K-edge. (b) The EXAFS fitting in K space at Fe K-edge. The best-fit structural parameters are listed in Supplementary Table 5.

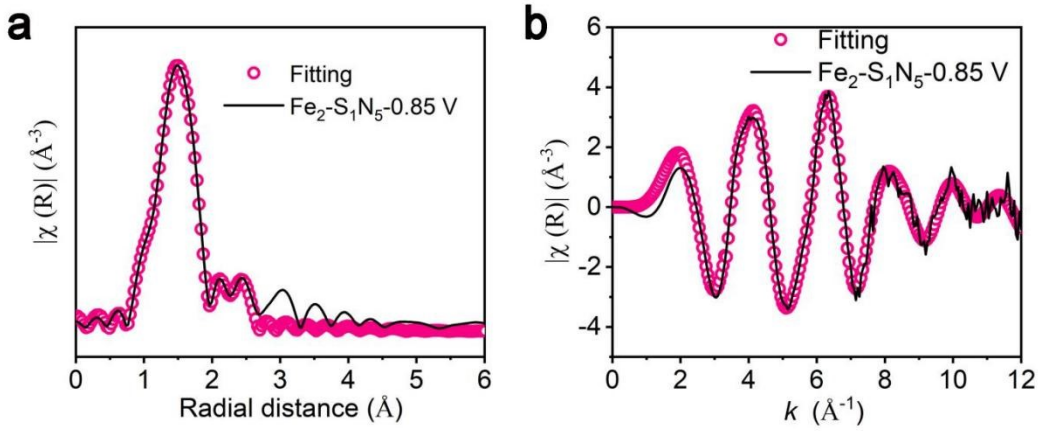

Figure S27 EXAFS fitting at 0.85 V vs. RHE. (a) The EXAFS fitting in R space at Fe K-edge. (b) The EXAFS fitting in K space at Fe K-edge. The best-fit structural parameters are listed in Supplementary Table 5.

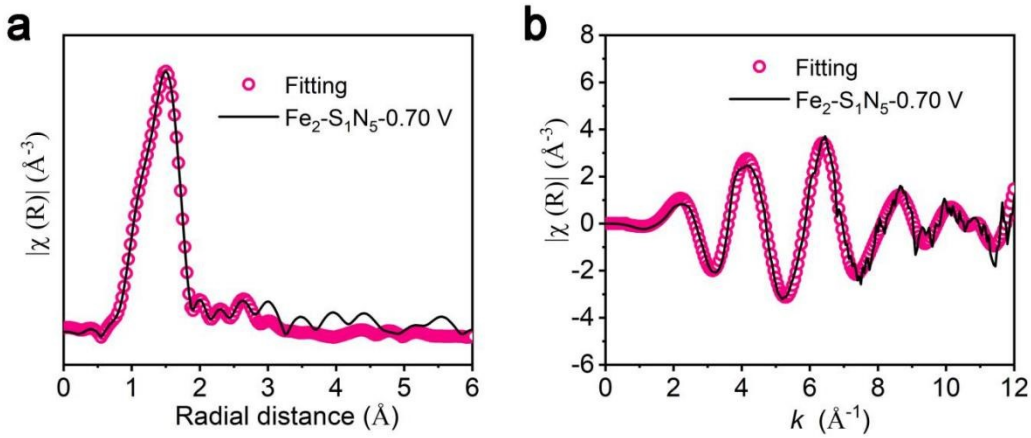

Figure S28 EXAFS fitting at 0.7 V vs. RHE. (a) The EXAFS fitting in R space at Fe K-edge. (b) The EXAFS fitting in K space at Fe K-edge. The best-fit structural parameters are listed in Supplementary Table 5.

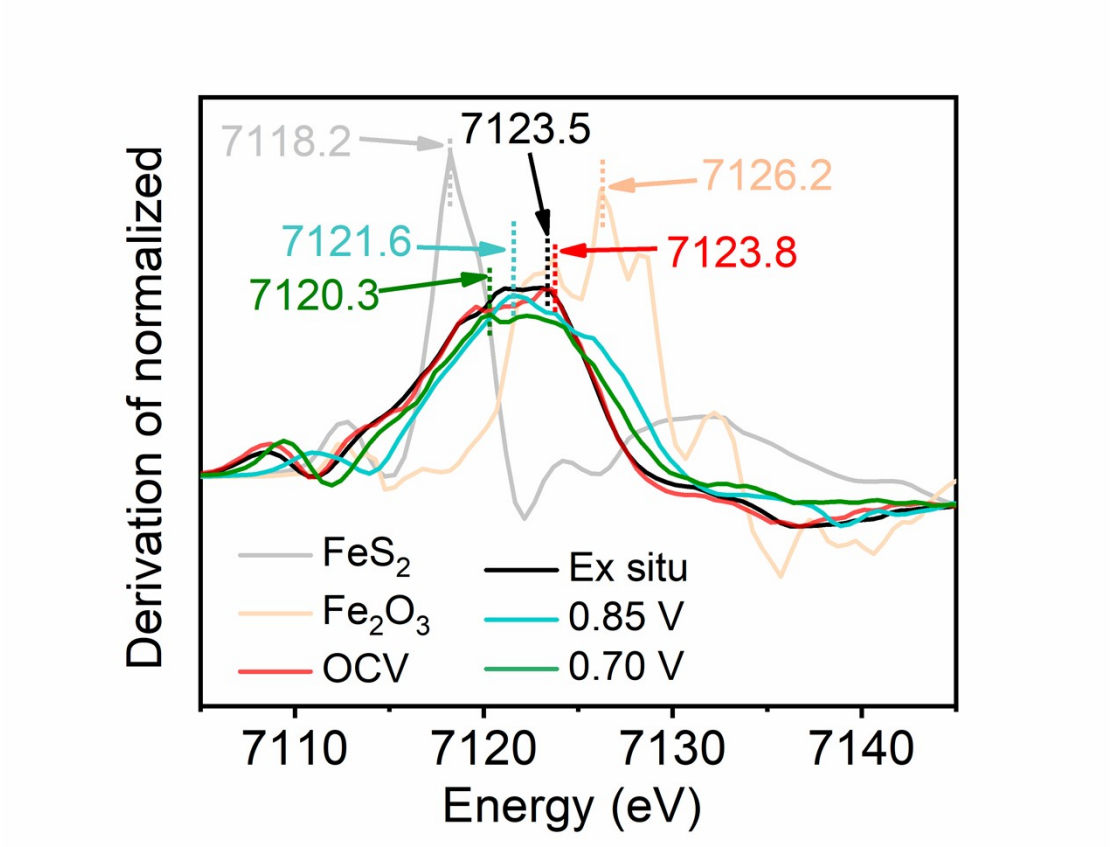

Figure S29 First-derivative XANES curves of Fe_2-S_1N_5/SNC under different potential.

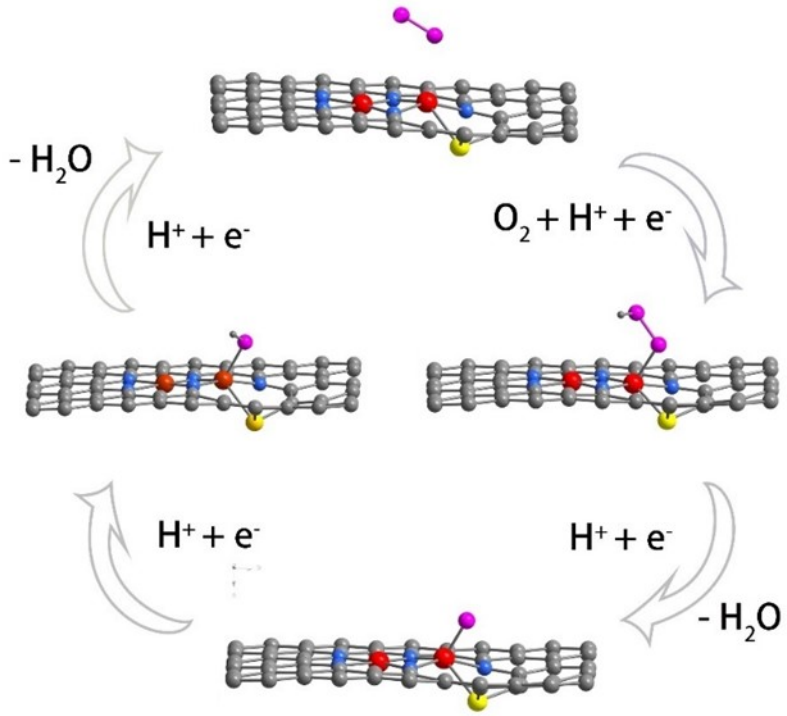

Figure S30 Demonstration of oxygen reduction path of catalyst Fe_2-S_1N_5/SNC (Path 1, Fe1).

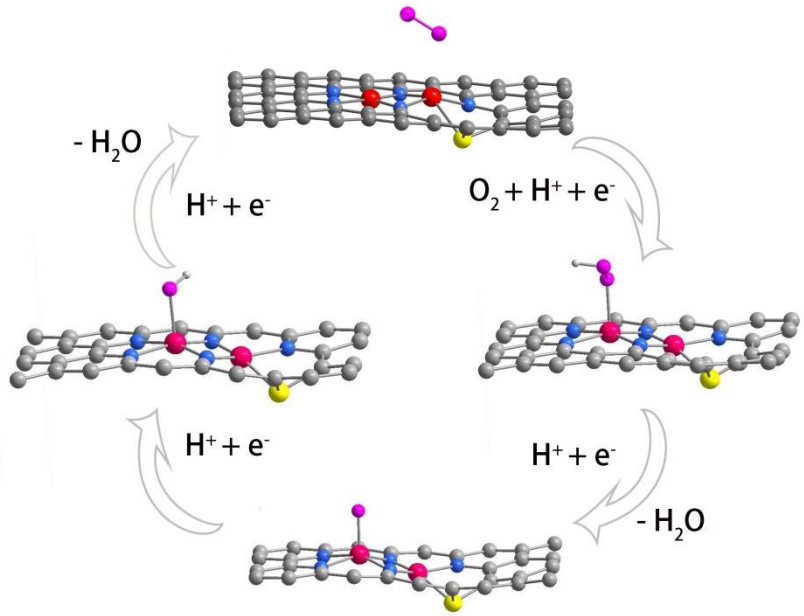

Figure S31 Demonstration of oxygen reduction path of catalyst Fe_2-S_1N_5/SNC (Path 2, Fe2).

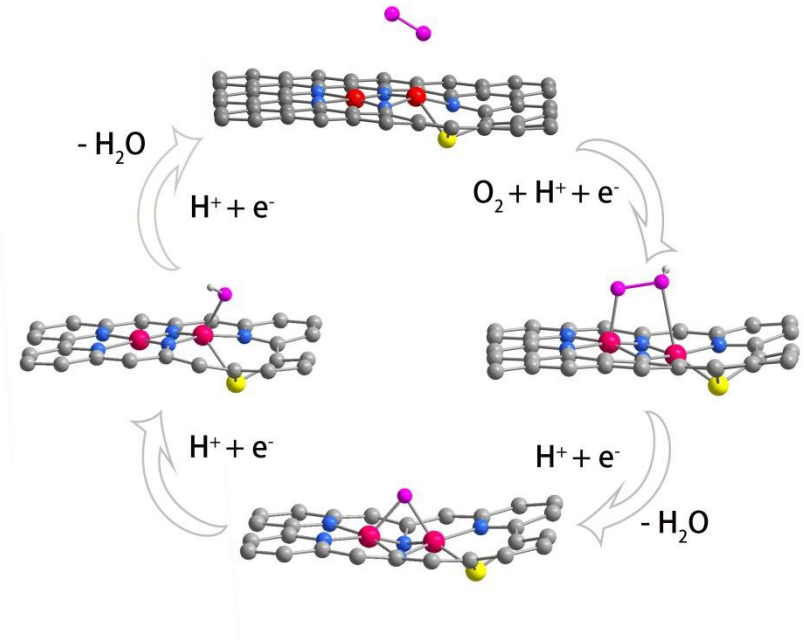

Figure S32 Demonstration of oxygen reduction path of catalyst Fe_2-S_1N_5/SNC (Path 3, Fe-Fe/Fe1).

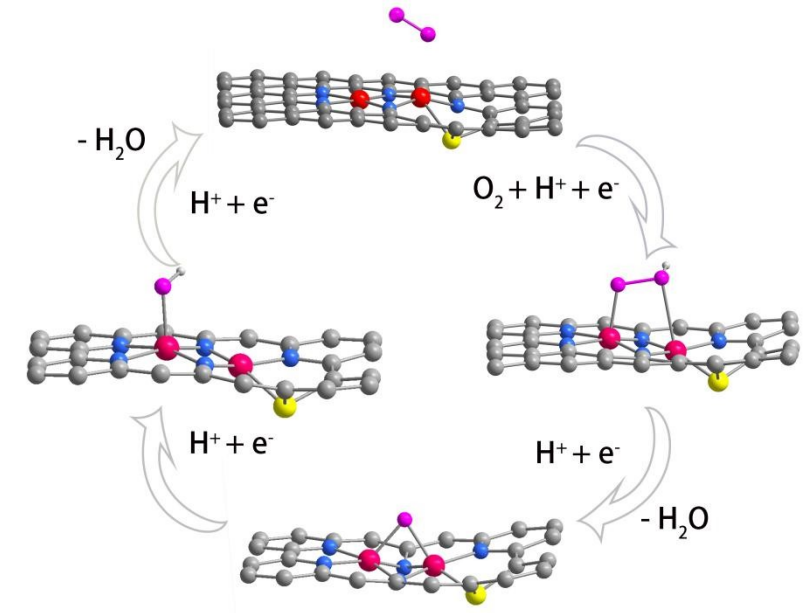

Figure S33 Demonstration of oxygen reduction path of catalyst Fe_2-S_1N_5/SNC (Path 4, Fe-Fe/Fe2).

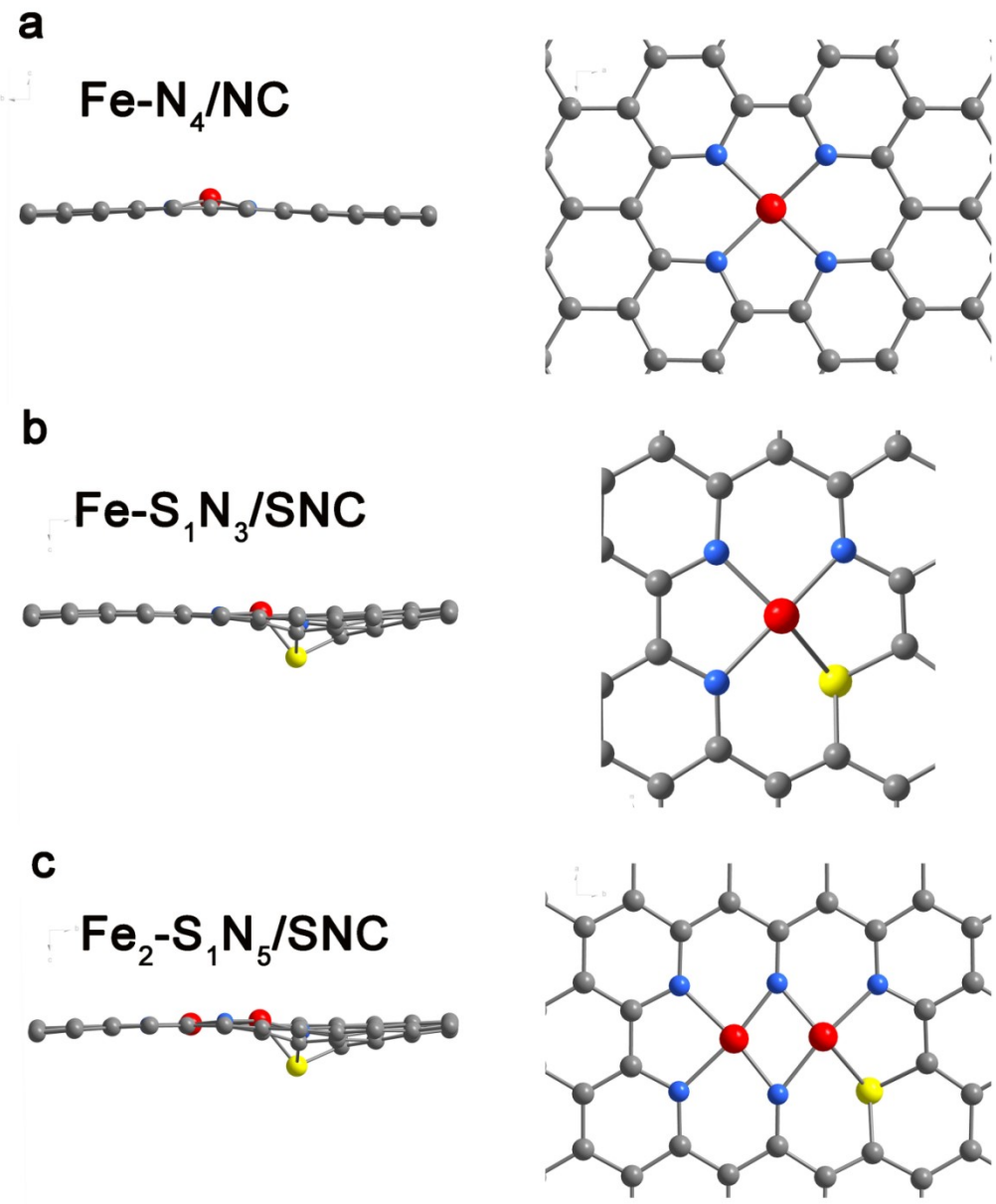

Figure S34 Optimized geometry of Fe-N_4/NC, Fe-S_1N_3/SNC, and Fe_2-S_1N_5/SNC.

Table S1. Summary on the surface areas, pore volumes of Fe-N_4/NC, Fe-S_1N_3/SNC and Fe_2-S_1N_5/SNC.

Sample	S_{BET} (m^2 g^{-1})	V_T(cm^3 g^{-1})
Fe-N_4/NC	95	0.31
Fe-S_1N_3/SNC	128	0.35
Fe_2-S_1N_5/SNC	104	0.26

Table S2. Structural parameters of Fe_2-S_1N_5/SNC extracted from the EXAFS fitting. (S_0^2=0.85)

Sample	Scattering pair	CN	R(Å)	$\sigma^2(10^{-3}Å^2)$	ΔE_0(eV)	R factor
Fe_2-S_1N_5/SNC	Fe1-N	3.0	1.99	5.3	2.0	0.005
	Fe2-N	3.9	1.96	5.4		
	Fe-S	0.9	2.24	4.9		
	Fe-Fe	1.1	2.46	7.1		
Fe-N_4/NC	Fe-N	3.9	1.97	7.9	1.5	0.007
Fe-S_1N_3/SNC	Fe-N	2.9	1.96	6.8	2.0	0.005
	Fe-S	1.0	2.25	7.6		

S_0^2 is the amplitude reduction factor; CN is the coordination number; R is interatomic distance (the bond length between central atoms and surrounding coordination atoms); σ^2 is Debye-Waller factor (a measure of thermal and static disorder in absorber-scatterer distances); ΔE_0 is edge-energy shift (the difference between the zero kinetic energy value of the sample and that of the theoretical model). R factor is used to value the goodness of the fitting.

* This value was fixed during EXAFS fitting, based on the known structure of Fe foil.

Error bounds that characterize the structural parameters obtained by EXAFS spectroscopy were estimated as N ± 20%; R ± 1%; σ^2 ± 20%; ΔE_0 ± 20%.

Table S3. Structural parameters of Fe_2-S_1N_5/SNC extracted from the EXAFS fitting. (S_0^2=0.85)

Sample	Scattering pair	CN	R(Å)	$\sigma^2(10^{-3}Å^2)$	ΔE_0(eV)	R factor
Fe_2-S_1N_5/SNC after ORR	Fe1-N	2.8	1.98	4.9	3.1	0.012
	Fe2-N	3.9	1.97	5.2		
	Fe-S	1.0	2.23	5.3		
	Fe-Fe	1.0	2.45	6.8		

S_0^2 is the amplitude reduction factor; CN is the coordination number; R is interatomic distance (the bond length between central atoms and surrounding coordination atoms); σ^2 is Debye-Waller factor (a measure of thermal and static disorder in absorber-scatterer distances); ΔE_0 is edge-energy shift (the difference between the zero kinetic energy value of the sample and that of the theoretical model). R factor is used to value the goodness of the fitting.

* This value was fixed during EXAFS fitting, based on the known structure of Fe foil.

Error bounds that characterize the structural parameters obtained by EXAFS spectroscopy were estimated as N ± 20%; R ± 1%; σ^2 ± 20%; ΔE_0 ± 20%.

Table S4. Structural parameters of Fe_2-S_1N_5/SNC extracted from the EXAFS fitting. (S_0^2=0.85)

Sample	Scattering pair	CN	R(Å)	$\sigma^2(10^{-3}Å^2)$	ΔE_0(eV)	R factor
Fe_2-S_1N_5/SNC at Ex stu	Fe1-N	3.1	1.98	5.3	2.0	0.005
	Fe2-N	4	1.97	4.7		
	Fe-S	0.9	2.24	4.9		
	Fe-Fe	1.1	2.45	7.1		
Fe_2-S_1N_5/SNC at OCV	Fe1- N	3.0	1.97	6.1	2.5	0.007
	Fe2- N	3.9	1.95	5.5		
	Fe-S	1.0	2.23	4.5		
	Fe-Fe	1.1	2.47	7.3		
Fe_2-S_1N_5/SNC at 0.85 V	Fe1- N	3.0	2.00	3.4	2.0	0.009
	Fe2- N	4.0	1.98	3.4		
	Fe-S	1.1	2.25	5.6		
	Fe-Fe	0.9	2.44	5.1		
Fe_2-S_1N_5/SNC at 0.70 V	Fe1- N	2.9	2.01	8.7	2.0	0.007
	Fe2- N	3.1	2.00	6.1		
	Fe-S	1.0	2.25	6.3		
	Fe-Fe	1.1	2.42	2.5		

$S0^2$ is the amplitude reduction factor; CN is the coordination number; R is interatomic distance (the bond length between central atoms and surrounding coordination atoms); σ2 is Debye-Waller factor (a measure of thermal and static disorder in absorber-scatterer distances); ΔE0 is edge-energy shift (the difference between the zero kinetic energy value of the sample and that of the theoretical model). R factor is used to value the goodness of the fitting.

Error bounds that characterize the structural parameters obtained by EXAFS spectroscopy were estimated as N ± 20%; R ± 1%; σ2 ± 20%; ΔE0 ± 20%.

Table S5. Comparison of the ORR electrocatalytic activity of Fe_2-S_1N_5/SNC and other catalysts reported in the literature under acid electrolyte.

Catalyst	Electrolyte	Halfwave potential (V vs. RHE)	Limitd current (mg cm^{-2})	Reference
Fe_2-S_1N_5/SNC	**0.1M $HClO_4$**	**0.829**	**5.82**	**This work**
Fe_1NGF	0.1M $HClO_4$	0.813	/	Nano Energy 114 (2023) 108647.
Fex/Cu-N@CF	0.1M $HClO_4$	0.815	/	Energy Environ. Sci.,2023,16,3576-3586.
FeMnac/Mn-N_4C	0.5 M H_2SO_4	0.79	5.38	Angew. Chem. Int. Ed. 2022, e202214988.
Fe-AC-CVD	0.5 M H_2SO_4	0.915	/	Nature Energy 2022, 7, 652.
Fe/Zn-N-C	0.1M $HClO_4$	0.808	/	Energy Environ. Sci., 2022,15, 1601-1610.
Fe, Mn/N-C	0.1M $HClO_4$	0.804	6.77	Nature Commun.2021, 12, 1734.
Fe-N_4-C	0.5 M H_2SO_4	0.74	/	Energy Environ. Sci., 2022,15, 1183-1191.
FeSA-N-C	0.1M $HClO_4$	0.80	5.60	Nat. Commun. 2020, 11, 2831.
Fe@ N_3C_1	0.1M $HClO_4$	0.76	/	Angew. Chem. Int. Ed. 2020, 59, 23678.
SAs@NCTCs	0.1M $HClO_4$	0.80	5.93	Appl. Catal. B: Environ. 313 (2022) 121464.

References

[1] Y. Hu, J. Zhang, T. Shen, Z. Li, K. Chen, Y. Lu, J. Zhang, D. Wang, *Adv. Mater. Interfaces.* **2021**, 13, 29551-29557.

[2] Y. Hu, X. Guo, T. Shen, Y. Zhu, D. Wang, *ACS Catalysis.* **2022**, 12, 5380.

[3] G. Kresse, J. Hafner, *Physical Review B.* **1993**, 47, 558.

[4] G. Kresse, J. Hafner, *Physical Review B.* **1994**, 49, 14251.

[5] P. E. Blöchl, *Physical Review B.* **1994**, 50, 17953.

[6] K. B. John P. Perdew, Matthias Ernzerhof, *Phys. ReV. Lett.* **1996**, 77, 3865.

[7] J. P. Perdew, W. Yue, *Physical Review B.* **1986**, 33, 8800.

[8] G. Kresse, *Physical Review B.* **1999**, 59, 1758.

[9] S. Grimme, *Journal of Computational Chemistry.* **2006**, 27, 1787.

[10] S. Grimme, J. Antony, S. Ehrlich, H. Krieg, *The Journal of Chemical Physics.* **2010**, 132.

[11] H. J. Monkhorst, J. D. Pack, *Physical Review B.* **1976**, 13, 5188.

[12] J. R. J. K. Nørskov, A. Logadottir, and L. Lindqvist, *J. Phys. Chem. B.* **2004**, 108, 17886.